Development of a Contra-Rotating Tidal Current Turbine and Analysis of Performance

J.A. Clarke, G.Connor, A.D. Grant, C.M. Johnstone, and D. Mackenzie

Energy Systems Research Unit, Department of Mechanical Engineering
75 Montrose Street, University of Strathclyde, Glasgow, UK
E-mail: Gary.Connor@strath.ac.uk

Abstract

The Energy Systems Research Unit within the Department of Mechanical Engineering at the University of Strathclyde has developed a novel contra-rotating tidal turbine. A 0.82 m diameter scale model has been built and tested in the University's tow tank, the results of which were used to inform the design and construction of a larger 2.5 m diameter prototype device. This prototype device has undertaken initial sea trials and the results are encouraging.

This paper reports the advantages of a contra-rotating marine turbine, the engineering design rationale, the testing programme undertaken in both the test tank and at sea, and how data from the test programme can be used to verify the design methodology. The paper concludes by reporting the progress being made towards the design and deployment of a grid-connected device.

Keywords: Tidal, marine, turbine, contra-rotating.

Nomenclature

C_P = power coefficient
a   = axial flow factor
γ = yaw angle
C_T = thrust coefficient
λ = tip speed ratio

Abbreviations
BEM   = Blade Element Model
CAD   = Computer Aided Design
CFD   = Computational Fluid Dynamics
CoRMaT = Contra Rotating Marine Turbine
FEA   = Finite Element Analysis
Rpm   = Revolutions per minute
TSR   = Tip Speed Ratio
UK   = United Kingdom

1   Introduction

It is widely accepted that tidal energy could have a substantial impact in meeting UK renewable targets [1]. However, the economics of tidal technology currently are not attractive within unsubsidised power markets. Table 1 lists the output energy cost (not including externalities) for a number of technologies, summarised by the UK Government [2] from reputable sources [3-5].

Technology	Cost £/MWh
Gas	20 – 23
Gas (CO_2 capture & storage)	35 – 37
Coal	36 – 39
Coal (CO_2 capture & storage)	57 – 61
Nuclear	25 – 40
Wind (onshore)	15 – 25
Wind (offshore)	20 – 30
Tidal	?

Table 1: Electricity production costs by generation technology.

It is notable that UK Government subsidies under the DTI Marine Development Fund can offer £100/MWh [6], plus monies for the Renewable Obligation Certificate (ROC) and Levy Exemption Certificate (LEC), totalling a minimum of around £137/MWh at present. This incentive is available to promising pre-commercial tidal devices for a limited period to bridge the pre-commercial and main-market gap. However in the medium term tidal technology will have to, as a minimum, compete with other renewable technologies if it is to successfully enter the renewable and conventional power markets.

2   Economics of Tidal Turbines

The economics of tidal technology are somewhat uncertain due to the fledgling market for devices, and limited experience in construction and operation over significant periods.

2.1   Moorings and Mounting

The probable major cost-categories associated with pile mounted tidal turbines are given in Figure 1. It is notable that a very large proportion of the cost for a pile-mounted turbine is associated with the structural steel elements (33%) and turbine installation (16%).

Further studies indicate similar orders of magnitude (33%) [7] for pile-mounted marine turbines, and indeed these proportions are comparable to those for offshore wind-turbine piled mountings: 25% and 28% of capital cost respectively [8]. Additionally around 52% of the UK resource is in deep (>40m) sites [9]

where piled structures are unlikely to be sufficiently economic. Thus lower cost options for deeper water should be considered.
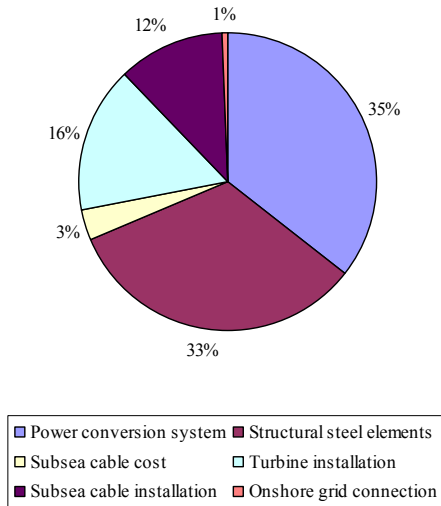
Figure 1: Estimated breakdown of costs for a farm of pile-mounted tidal turbines [10].

2.2 Counter-acting Reactive Torque

All rotating systems produce reactive torque which in the case of a marine turbine rotor produces a requirement for a structure, mooring or a further contra-rotating rotor to react against the initial rotational torque. The first two options incur significant additional expense with no additional offsetting power gain compared to a contra-rotating dual rotor design. All contra-rotating designs to date contain rotors laterally adjacent to one another and connected by a spar.

Studies of tidal streams [11] would indicate that large shear or turbulence effects are present over small distances, and are therefore likely to produce unequal forces on each of the two adjacent rotors, thus creating a yawing moment that must be counteracted by the supporting structure or mooring. Such a mooring must therefore be fixed at 2 points, which limits tidal flow direction tracking. There is also the matter of dynamic loading: misalignment will introduce cyclic loads on the blades which may result in yaw oscillations if not restrained. Finally, unwanted yaw misalignment will degrade energy capture proportionately to the square of the cosine of the yaw angle [12]:

$$C_P = 4a(\cos\gamma - a)^2.$$

3 CoRMaT Design Philosophy

Thus with regard to the aforementioned economics there emerges the practical possibility of a marine current turbine with in-line contra-rotating rotors to specifically reduce the issue of high capital costs, by conferring:

- Near-zero reaction torque on the supporting framework, reducing the structural and mooring elements, and thus cost.
- Reduced wake swirl, giving increased power capture and lower environmental impact.
- Higher relative shaft rotational speeds, simplifying or eliminating the gear-train. (After blades, the gearbox is the second least reliable component of a wind turbine [13]). Similar considerations are likely with marine current turbines.

The design and construction of a Contra Rotating Marine Turbine (CoRMaT) is hereafter described.

4 Design and Testing at 1/30th Scale

4.1 Rotor Hydrodynamic Design

Turbine design is more fully described in [14-15]. In summary, an extension of conventional blade element momentum (BEM) theory was used to predict the geometry of the downstream rotor relative to the specified upstream rotor. A dissimilar number of blades was chosen for the two rotors (3 on the upstream rotor, 4 on the downstream rotor) to minimise stall and dynamic interactions during operation. The aerofoil section used for both rotors was the NREL S814 [16].

4.2 Rotor Design for Torque Matching

A condition of zero net torque was imposed under all design circumstances, the torques exerted on each of the two rotors by the flowing stream being equal and opposite. The rotor was designed to produce equal torque and equal axial thrust on each rotor for the condition $\lambda_1 = \lambda_2 = 3$. The design produced was then scrutinised by a different BEM code, which predicted the equal torque condition at $\lambda_1 = 3$, $\lambda_2 = 2.875$ with an axial thrust distribution of 51% / 49% for the upstream and downstream rotors respectively: an acceptable validation of the design process.

4.3 1/30th Scale Tow-Tank Testing

A 1/30th scale CoRMaT model was built and underwent trials to substantiate the contra-rotating design predictions with regard to C_p, loadings and reactive torque balancing.

To meet the condition of zero net torque, the same brake load had to be applied to each rotor; however, it was important that the rotors were free to turn at different speeds. A differential gearbox was constructed to meet these criteria and frictional load was applied by a small disc brake, hydraulically actuated.

4.4 Results from 1/30th Scale CoRMaT

The values of power coefficient as a function of tip speed ratio for differing blade pitch angles are shown

in Figure 2. As can be seen the experimental results from the 0.82m diameter tow-tested device with the closest rotor spacing (60mm) are in excellent agreement with those from the mathematical model.
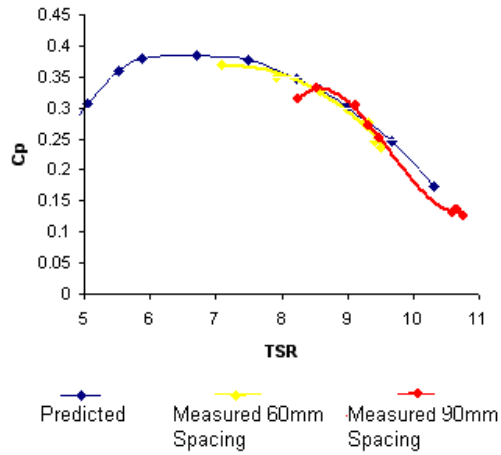
Figure 2: Tip Speed Ratio v. Coefficient of Performance for nominal blade pitch and 2 rotor spacing.
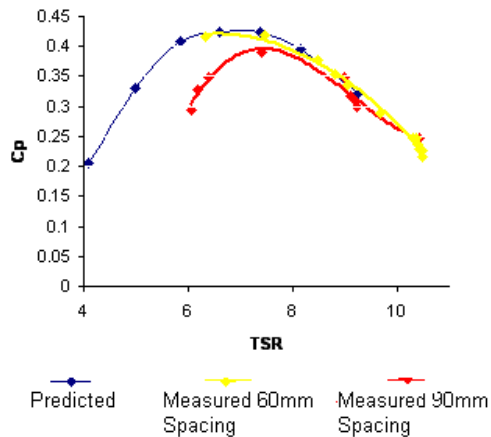
Figure 3: Tip Speed Ratio (TSR) vs. power coefficient (C_P) for +2°/+2° blade pitch angles and differing rotor spacing.

4.5 Discussion

A secondary variable, distinctive to a contra-rotating turbine, is that of inter-rotor spacing. The rotor design assumed that the rotors are in close proximity, and function as a single actuator disc as far as blade element theory is concerned. Correct inter-rotor spacing is therefore critical to ensure efficient operation of the overall system through minimisation of swirl and wake turbulence.

Figures 2 and 3 detail the effects of variation in blade spacing to achieve a good match between rotor sets. A reduction in performance is noted when the blade spacing is increased beyond the designed 60mm (0.073 rotor diameters) to 90mm.

The 1/30th scale testing verified the hydrodynamic design principles and provided confidence that the advantages of a contra-rotating turbine were realisable.

5   Turbine Design at 1/10th Scale

The test-tank results provided confidence to proceed with a larger 2.5m diameter sea-going 1/10th scale turbine. This prototype was designed in a similar manner to the tow-tank model [14].

The same fundamental concept as before, with 3- and 4-bladed rotors upstream and downstream, respectively was selected. Also as before, the NREL S814 aerofoil profile was used for both rotors. The design process followed the procedures established for the original 1/30th scale model.

Performance predictions for the turbine are given in [15]; as in the original small model, provision is made for adjusting the blade pitch.

Two areas are of specific importance with regard to the larger scale rotor: reduction of wake by rotor interaction: mechanical strength and structural integrity of the blades. The investigation of these facets is now described in greater detail.

5.1   Computational Fluid Dynamic Analysis

Computational Fluid Dynamic (CFD) work was progressed to further investigate wake reduction and interblade-spacing optimisation for the contra-rotating turbine. Figure 4 illustrates the reduction in turbulence intensity for a simple dual rotor as compared to a single rotor. This not only provides the aforementioned efficiency increase, but also reduces the wake and hence environmental impact.
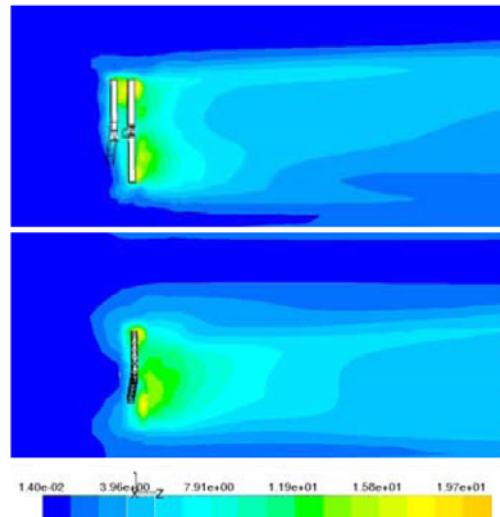
Figure 4: Simple FLUENT CFD comparison of vorticity for a dual and single rotor tidal turbine in a tidal stream of 1.5ms^{-1} velocity.

5.2 Blade Structural Analysis

The mechanical performance of the larger 1/10th scale turbine blade was assessed by Finite Element Analysis (FEA) to ensure sufficient strength for the forces encountered, and with regard to fatiguing.

Several models were produced as the design developed, the final comprising three integrated components, namely: the spar, the outer skin, and the solid fill.

The stepped stainless steel spar was modelled using 3 node beam elements beam189 with ANSYS [17].

The solid volume of the turbine blade was modelled as a 3D volume and meshed using 10 node isoparametric tetrahedral solid elements, solid92. The trailing edge of the blade is truncated to minimise meshing problems. The effect of this approximation on the structural response will be negligible. The solid volume of the blade is formed from a fill of microballoons and very slow epoxy resin. Isotropic resin material properties were assumed.

The outer skin was modelled using 8 node quadrilateral shell elements degenerated into 6 node triangular shell elements, shown in Figure 5. The outer skin consists of an anisotropic glass-carbon-epoxy composite. This complex material was approximated by a similar isotropic shell layer bonded to the fill material.
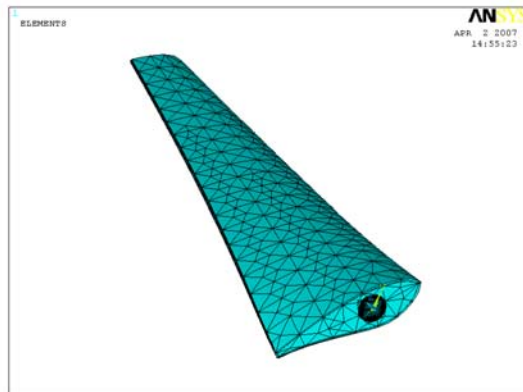
Figure 5: Blade skin degenerated into 6 node triangular shell elements.

The model is fixed at the base of the spar. Tangential and radial loads corresponding to the loading at tidal speeds of 5ms^{-1} as calculated by BEM are applied as distributed nodal forces.

A contour plot of the von Mises equivalent stress in the stainless steel spar for the non-skinned blade is shown in Figure 6. The maximum stress is 86.7MPa.

A contour plot of the von Mises equivalent stress in the fill material for the non-skinned blade is shown in Figure 7. The stress levels in the blade are an order of magnitude lower than those in the spar, which is the load bearing member transmitting the hydrodynamic forces to the hub of the rotor.
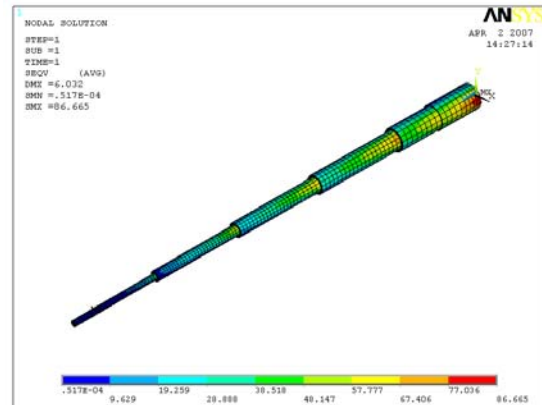
Figure 6: Stainless steel spar – von Mises equivalent stress.
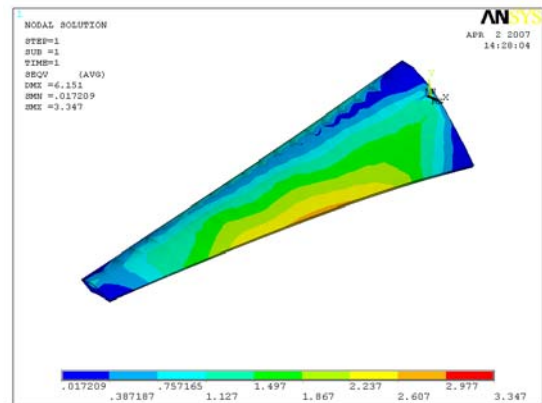
Figure 7: Internal blade fill – von Mises equivalent stress.

When the outer skin is applied, the stress in the spar reduces very slightly but the maximum stress remains at the root of the spar. The von Mises equivalent stress distribution at the surface of the skinned blade is shown in Figure 8. The stress remains at low levels throughout the blade, with a maximum value where the skin is connected to the spar.

The FE models created during the design process were used to guide the evolution of the design. However, the models created are based on a number of simplifying assumptions applied during the design process. The spar component of the model consists of several isotropic stainless beam elements of different diameter. This model would be expected to be relatively accurate in comparison with beam theory but the model does not evaluate the stress at the discontinuities in the spar where a large radius cutter was used. These stresses would be significant in fatigue assessment and are undergoing more detailed analysis.
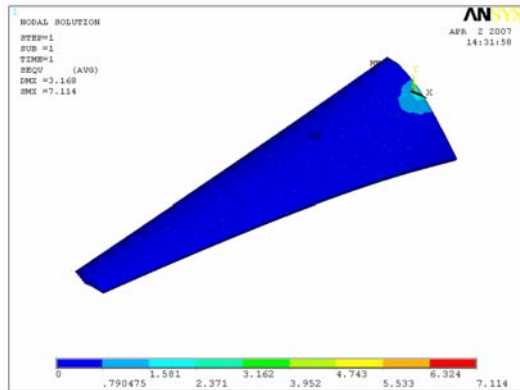
Figure 8: Composite blade – von Mises equivalent stress.

Approximate bulk isotropic material properties typical of the resins and fibres used were applied in the analysis. The calculated stresses are therefore approximate and average in nature. The model does not calculate important parameters such as inter-laminar shear stress, however, the results of analyses of different configurations were sufficient to guide the design process and produce robust rotor blades that proved their reliability during the sea trials.

Future work on larger, more safety critical turbines with specified design (fatigue) life requirements will require more detailed and complex finite element analysis than presented here. The required modelling technology is currently available and does not present a substantial problem. Further in-depth analysis of blade design, materials, structural integrity and longevity in the hostile marine environment is currently being undertaken with a number of partners
.

6   Power Take-off

CoRMaT was due to be tested during the summer of 2006, however external issues prevented this. Firstly, the carbon fibre required for structural integrity of the blades was delayed due to world-wide rationing of the material. Secondly, the original design necessitated the boring of a hollow drive shaft to allow the use of two concentric shafts (one from each rotor); unfortunately local manufacturing capacity was limited due to a large demand for high-value oil and earthmoving components. Both delays necessitated major design modifications to produce CoRMaT within the project timescales.

The simplified design utilised a single stationary shaft, or spine, on which where mounted the two independent sets of rotors and their associated power take-offs and instrumentation. Figure 9 refers. This arrangement allowed flexible control, monitoring and spacing of the two separate rotors.
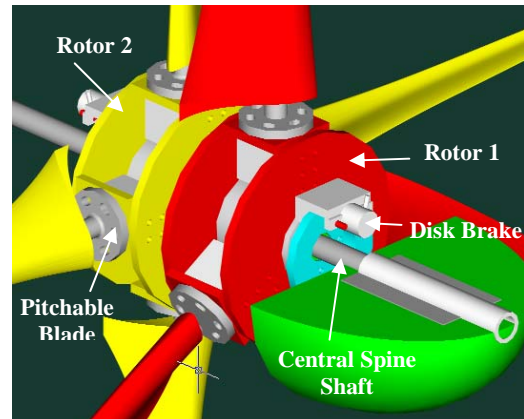
Figure 9: CAD drawing of modified double rotor and power take-off configuration

Power take-off is by dual independently actuated, rotor mounted, hydraulic disc brakes to provide a highly controllable system even at very low TSR for experimental purposes. The power from each rotor was derived from the torque measured at each brake calliper by a load-cell, while the rotational speed was measured by a shaft tachometer on each rotor. Figure 10 refers.
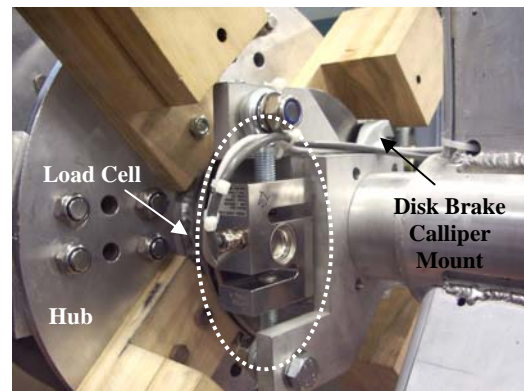
Figure 10: Rear rotor showing power take-off and instrumentation

7   Frame and Instrumentation

Figure 11 is a CAD rendering of the turbine and its support frame. The support frame was constructed from welded alloy box section, with stainless steel reinforcement and cathodic protection.

The limiting factor in CoRMaT frame design was the vessel (the St. Hilda – a Miller Fifer 52') available to undertake the testing within budgetary limits, which had a maximum lift capacity of 1 tonne. The frame was only necessary during this early development phase: to provide a stable platform for lifting and sea transport on-deck, to provide protection should the turbine require to be abandoned to the seabed during

testing, and to provide the mounting points for cameras and instrumentation.
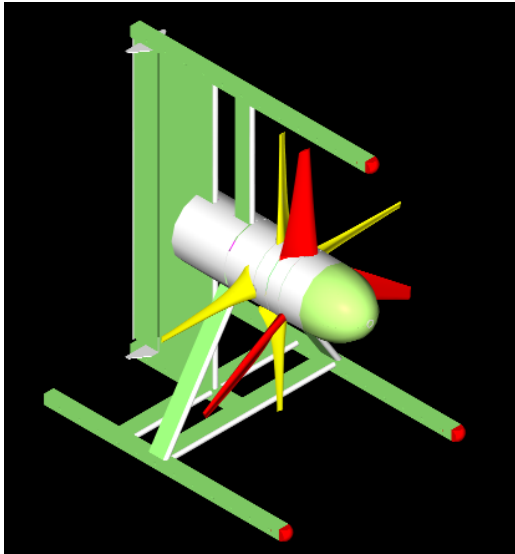
Figure 11: CAD drawing of turbine showing frame mounting.

The tail was added to provide stability and off-centre yaw angles for experimentation, however, its use was later found not to be required under normal operational conditions. The entire turbine, including frame and all umbilicals weighed a total of 663kg in air.

8   Sea Tests at 1/10th Scale

Due to project delays and funding deadlines the sea-trials were undertaken in November 2006 during a long period of less than tranquil conditions (winds generally above Force 6, peaking at Force 10 with only short intervals of calmer weather).

Figure 12: CoRMaT on frame aside the St Hilda (nacelle cowling removed)

The original plan had been to test the device in a tidal race between 2 islands on the west coast of Scotland, however the prevailing stormy weather and the vessel selected to conduct the tests made this impossible to achieve in safety. Instead the turbine was mounted to the bow-side of the vessel and towed while well submerged through the water within the more sheltered confines of the Holy Loch in the Clyde approaches (Figure 12).

9   Results from Sea Trials

9.1 Measured Data

The sea trials although limited in scope provided good power take-off and blade loading data for lower 'tidal' speeds.

CoRMaT functioned according to expectations, reflecting the predicted power curves over the limited tidal speed range simulated by towing. The maximum towing speed achievable was $1.5ms^{-1}$ before the St Hilda became un-manoeuvrable. 2098W was recorded at $1.5ms^{-1}$ equating to a C_p of 0.38. CoRMaT was designed to operate in tidal currents up to at least $3.5ms^{-1}$, producing 42kW.

Due to limitations of the hydraulic control system, torque matching between the two rotors was difficult to achieve for long periods, however sufficient proof of this ability was obtained via the load cells to confirm the cancellation of reactive yawing under normal operating conditions.

Dynamic blade loading data was recorded at 1 kHz (minimum angular loading resolution of 0.7 degrees) from marine grade full-bridge temperature compensated strain gauge arrays, by in-hub solid-state 'CF' memory data recorders. Figures 13 demonstrates data downloaded from the two hub data recorders, and reveals the reduced dynamic (shock) thrust loadings on the downstream rotor when both rotors are contra-rotating as designed.
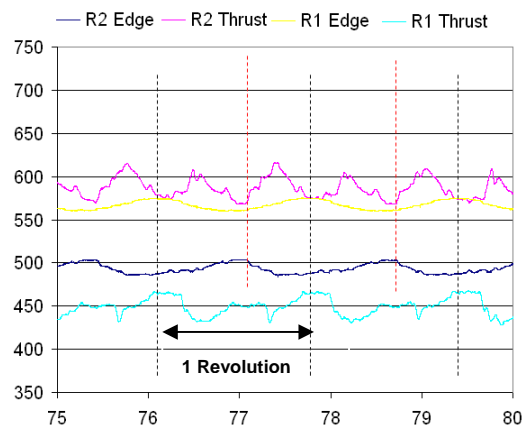
Figure 13: Blade thrust and edgewise loadings (arbitrary units) recorded over time: both rotors contra-rotating.
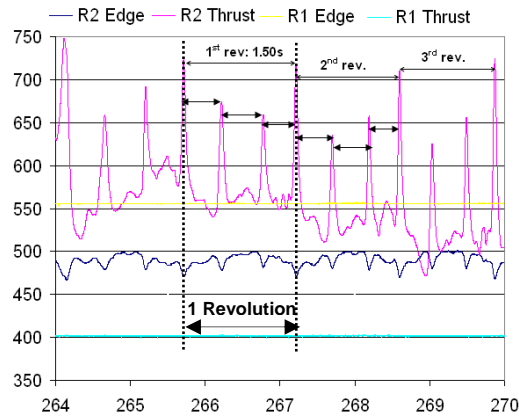
Figure 14: Blade thrust and edgewise loadings (arbitrary units) recorded over time:: front rotors stationary, downstream rotating.

Figure 14 is a recording during the same test-run under similar conditions to those in Figure 13, except that the upstream rotor (R1) has been stopped.

9.2 Discussion
In the test depicted in Figure 13, the speeds of the two rotors are nearly equal. The shaft torques are also similar, but not identical: the comparison here is between 3 times the R1 edge loading, and 4 times the edge load for R2. Both edge traces show a once-per-revolution ripple from gravitational effects.

The upstream rotor R1 experienced periodic falls in its thrust loading due to interference from the front support frame (seen in Figure 12), which remained in place during this test. The wakes from the two lower arms of the frame seem to have merged to some extent.

The downstream rotor R2 would be expected to show signs of disturbance from the 3-bladed rotor immediately upstream, at a frequency of $3(f_1 + f_2)$, where f_1 and f_2 are the rotational frequencies of the two rotors. In this case where f_1 and f_2 are similar, disturbances should come approximately 6 times per revolution. However, the thrust trace for R2 (Figure 13) seems to be dominated by a twice-per-revolution effect, suggesting that (as for R1) the support frame was the culprit. It is difficult to detect any regular disturbances for R2 at a higher frequency.

With rotor 1 stalled (Figure 14) disturbances to rotor 2 should occur 3 times per revolution, and this effect is clearly visible for both thrust and edge loads. The interesting feature is the magnitude of cyclic thrust loadings produced in passing through the wakes of the stationary blades. The conclusion from these tests is that wakes from stationary bluff bodies are potentially far more serious than the blade / blade interactions in a properly functioning contra-rotating turbine: to the extent of an order of magnitude in the cases presented here. The consequences for rotors operating in close proximity to supporting structures are clear to see.

The data obtained from tank tests and sea trials suggest that it is possible to produce a contra-rotating marine turbine with hydrodynamically matched rotors, producing relatively small blade interaction loads.

10   Further Work

The work on CoRMaT continues with development in a number of specific areas:

- Further testing of CoRMaT and refinement of its systems in a tidal stream over an extended period of 8 months.
- Installation of a complete electrical power take-off utilising direct-drive induction machinery and power conditioning to provide grid-compliant power.
- Further flume and tow-tank tests with respect to the stability and dynamic properties of moored and freely 'flying' turbines.
- Continued analysis and testing programme for rotor blade materials to provide structural integrity and resistance to the harsh marine environment.

11   Conclusions

The benefits of a contra-rotating marine current turbine have been described and demonstrated with reference to scaled tow-tank testing and sea-trials.

The experimental results confirm that it is possible to offset marine turbine reactive torque (and hence mooring cost) by means of contra-rotation, although further work is required to prove the robustness of the sea-going prototype's active hydraulic control.

Power take-off data is in excellent agreement with the predicted C_p values calculated by modified BEM codes, for both the $1/30^{th}$ and $1/10^{th}$ scale CoRMaT. Power output data from the $1/10^{th}$ scale CoRMaT was however limited by the weather during the test period, and further testing in higher tidal currents is scheduled to produce further confirmation of performance.

Acknowledgements

References

[1] Black & Veatch, 18th July 2005: *UK Tidal Stream Energy Resource and Technology.* Summary Report for the Carbon Trust.
www.thecarbontrust.co.uk/ctmarine3/res/PhaseIITidalStreamResourceReport.pdf.

[2] Performance and Innovation Unit (PIU), 2001: *UK Energy Review.*
http://www.piu.gov.uk/2002/energy/report/index.htm

[3] Future Energy Solutions, 2003: *Analysis for Energy White Paper, using the MARKAL Model.*
http://www.dti.gov.uk/files/file10719.pdf
TSO, ISBN 0-10-157612-9

[4] UK Interdepartmental Analysts' Group. DTI, DEFRA, DfT, Treasury, Carbon Trust and Energy Savings Trust. 2001.

[5] UK DTI, January 2006: UK Energy Review Consultation Document. Annex B, pg 70.

[6] UK DTI, May 2005: *Marine Renewables Wave and Tidal-stream Energy Demonstration Scheme*.
www.dti.gov.uk/files/file23963.pdf

[7] C.J. Day Associates, 2001: *Tidal Turbine Installation at Fixed Navigation Marks*. DTI ETSU Report ETSU T/05/00214/REP DTI/Pub URN 01/1516.

[8] S. Rahman, G. Hagerman, 7th September 2006: *Wind Energy: Opportunities and Challenges for Offshore Applications*. Presentation to IEEE, Virginia Tech.

[9] Black & Veatch, 18th July 2005: *UK Tidal Stream Energy Resource and Technology.* Summary Report for the Carbon Trust.

[10] M. Previsic, June 10th 2006: System *Level Design, Performance, Cost and Economic Assessment - San Francisco Tidal In-Stream Power Plant*. EPRI.

[11] S.J. Couch, I. Bryden, 2006: *"Tidal Current Energy Extraction: Hydrodynamic Resource Characteristics",* Proceedings of the Institution of Mechanical Engineers, Part M: Engineering for the Maritime Environment, pp 185-194, ISSN 1475-0902.

[12] W.M.J. Batten, A.S. Bahaj, A.F. Molland, J.R. Chaplin, March 2007: *Power and Thrust Measurements of Marine Current Turbines under various Hydrodynamic Flow Conditions in a Cavitation Tunnel and Towing Tank.* Renewable Energy 32 (3), pp 407-426. Elsevier.

[13] S. Vittal and M. Teboul, 2004: *Performance and Reliability Analysis of Wind Turbines using Monte Carlo Methods based on System Transport Theory.* American Institute for Aeronautics and Astronautics.

[14] J.A. Clarke, G Connor, A D Grant and C M Johnstone, May 2007: *Design and testing of a contra-rotating tidal current turbine.* IMechE Journal of Power and Energy, Special Edition on Tidal Energy.

[15] J. A. Clarke, G. Connor, A. D. Grant, C. M. Johnstone and D. Mackenzie, 19 -25 August, 2006: *Design and initial testing of a contra-rotating tidal current turbine.* Proceedings of the World Renewable Energy Congress 2006, Florence, Italy.

[16] Somers D M, 1997: *Design and experimental results for the S814 airfoil.* Airfoil Incorporated, State College Pennsylvania, Subcontractor report NREL/SR-440-6019.

[17] ANSYS Version 10, ANSYS Inc., Canonsberg, PA 15317; 2005.